Robotica (2011) volume 29, pp. 211–219. © Cambridge University Press 2010
doi:10.1017/S0263574710000056

# Experimental backlash study in mechanical manipulators

Miguel F. M. Lima†*, J. A. Tenreiro Machado‡ and Manuel Crisóstomo§

†*Department of Electrical Engineering, Superior School of Technology, Polytechnic Institute of Viseu, 3504-510 Viseu, Portugal*
‡*Department of Electrical Engineering, Institute of Engineering, Polytechnic Institute of Porto, 4200-072 Porto, Portugal*
§*Institute of Systems and Robotics, Department of Electrical and Computer Engineering, University of Coimbra, Polo II, 3030-290 Coimbra, Portugal*

(Received in Final Form: February 3, 2010. First published online: March 4, 2010)

**SUMMARY**
The behavior of mechanical manipulators with backlash is analyzed. In order to acquire and study the signals an experimental setup is implemented. The signal processing capabilities of the wavelets are used for de-noising the experimental signals and the energy of the obtained components is analyzed. To evaluate the backlash effect upon the robotic system, it is proposed an index based on the pseudo phase plane representation. Several tests are developed that demonstrate the coherence of the results.

## 1. Introduction

Robotic systems have nonlinearities in the actuators that include deadzone, backlash, and saturation. This problem is particularly important in robotic manipulation where high precision is needed. In fact, the backlash is one of the most important nonlinearities that limit the performance of the mechanical manipulators. This dynamic phenomenon has been an area of active research, but due to its complexity well-established conclusions are still lacking.

The backlash in robotic systems has two main aspects: the identification and the control. Several authors have addressed the problem of identification.[1–6] Dagalakis and Myers[1] proposed a technique based on the coherence function to detect backlash in robotic systems. Another technique, proposed by Stein and Wang,[2] was based on the analysis of momentum transfer for detecting the backlash in mechanical systems. There have been also efforts toward the backlash detection using artificial intelligence schemes and state space observers.[4,5] Trendafilova and Brussel[6] present several tools to analyze the nonlinear dynamics of the robot joints.

To mitigate the effects of the backlash, several authors studied the control of the mechanical systems with this nonlinearity.[7–9] Nordin and Gutman[8] presented a survey of the techniques for controlling mechanical systems with backlash. The techniques included the use of linear controllers, such as proportional–integral–derivative controller (PID), state feedback, and observer-based algorithms. A control using the describing function, which is a common method for the analysis and synthesis of nonlinear systems, was also adopted.[7] Nonlinear,[10] neuro,[11] and fuzzy[12] controllers have been also proposed. More recently, the fractional order controllers were also applied to suppress the backlash in mechanical systems.[9] The problem of reducing the effects of backlash was also studied in other robotic applications, including systems with joint[13] and link[14] flexibility, in grippers,[15] and anthropomorphic hands.[16]

Modern robots use precision gears to reduce backlash. However, its elimination may be impracticable, because there are several sources of the effect which are impossible to remove completely.[1] Therefore, in order to reduce the backlash and its effects, a good understanding of this phenomenon is needed. In this perspective, we investigate the behavior of a mechanical manipulator with backlash in the joints.

Bearing these ideas in mind, this paper is organized as follows. Section 2 describes briefly the robotic system used to capture the signals. Sections 3 and 4 present some fundamental concepts, and the experimental results, respectively. Finally, Section 5 outlines the main conclusions and points out the plans for future work.

## 2. Experimental Platform

In order to analyze signals that occur in a robotic manipulator was developed an experimental platform. The platform has two main parts: the hardware and the software components.[17] The hardware architecture is shown in Fig. 1 (left). Essentially it is made up of a mechanical manipulator, a computer, and an interface electronic system. The interface box is inserted between the arm and the robot controller, in order to acquire the internal robot signals. The interface system captures also external signals, such as those arising from accelerometers and force/torque sensors. The modules are made up of electronic cards specifically designed for this work. The function of the modules is to adapt the signals and to isolate galvanically the robot's electronic equipment from the rest of the hardware required by the experiments.

The software package runs in a Pentium 4, 3.0 GHz PC and, from the user's point of view, consists of two applications. One, the acquisition application, is a program made up of

* Corresponding author. E-mail: lima@mail.estv.ipv.pt

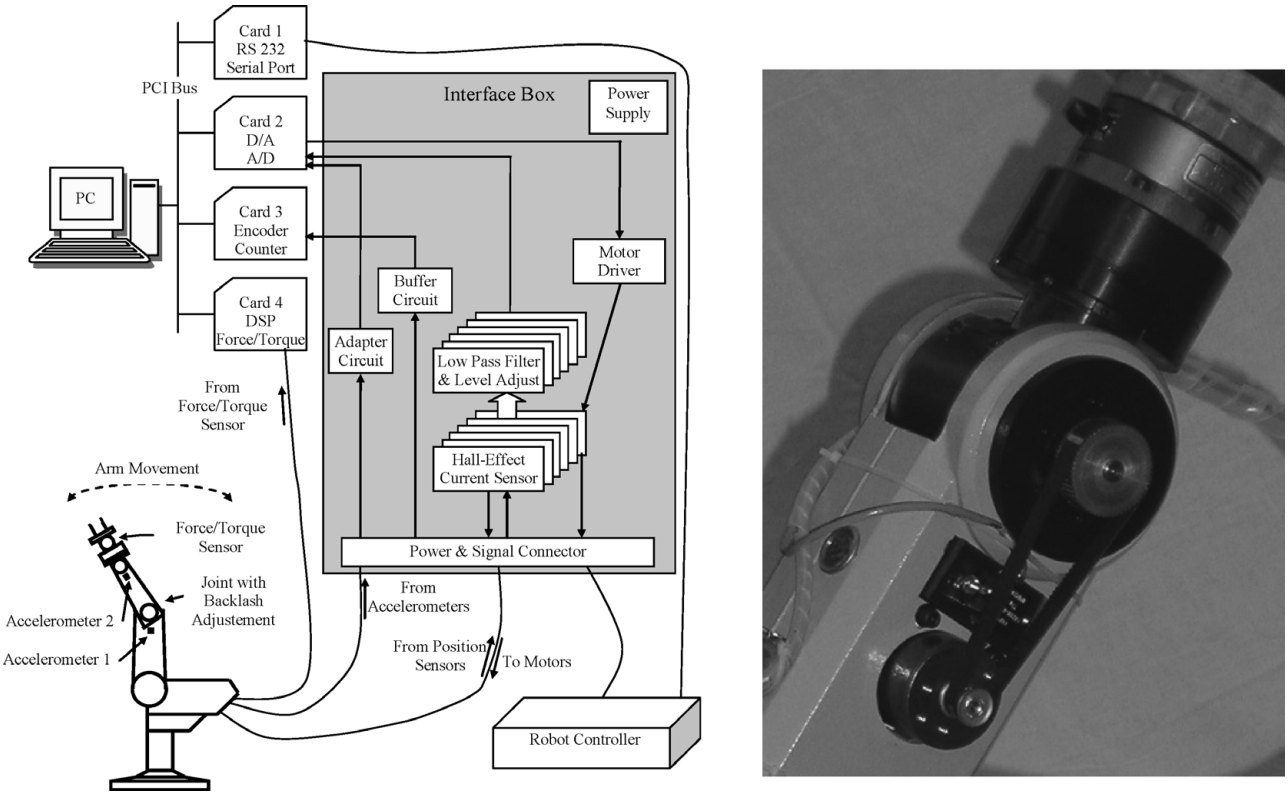


Fig. 1. Block diagram of the hardware architecture (left) and accelerometer 2 mounted on the robot arm (right).

two parts: the graphical user interface (GUI) module and the real time module. The other application is an Analysis Package that analyses the data obtained and recorded by the acquisition application. The real time software, running in the Hyperkernel, was developed in C based on a standard Windows NT/2000 development tool (MS Visual Studio) and the robot controller software was implemented in the advanced control language (ACL) proprietary language. The Windows NT/2000 Software is made up of the GUI module of the acquisition system and Analysis Package. The acquisition system software was developed in C++ with MS Visual Studio. The Analysis Package, running off-line, reads the data recorded by the acquisition system and examines them. The Analysis Package allows several signal processing algorithms such as, Fourier transform, correlation, time synchronization, etc. With this software platform both the Hyperkernel and the Analysis Package tasks can be executed on the same PC.

The manipulator is a vertical articulated robot with five rotational joints. The third joint connects the upper arm to the forearm of the robot. This joint is driven through a servomotor coupled to the harmonic drive gear by a timing belt. By adjusting the belt tension of the third joint two-stage transmission, three distinct degrees of backlash were introduced that are qualitatively classified as: (i) low backlash, (ii) medium backlash, and (iii) high backlash. The vibration response is measured with the accelerometers 1 and 2 that are mounted in the end of the upper arm and forearm, respectively (see Fig. 1). The robot motion is programmed in a way such that only the third joint is driven and, consequently, it oscillates over a predefined range from the vertical position. The axis of the rotational joints 2, 3, and 4 are parallel; therefore, the effects of the third axis rotation affect directly the adjacent joints. During the motion several signals are recorded with a sampling frequency of $f_s = 750$ Hz. The tests developed show that this sampling frequency is adequate to capture the relevant dynamic behavior of the system. The signals come from different sensors, such as accelerometers, wrist force and torque sensor, position encoders, and joint actuator current sensors. Figure 1 (right) depicts the accelerometer 2 mounted on the robot arm.

## 3. Main Concepts

This section presents briefly the fundamental concepts involved in the experiments. In order to deal with the noisy signals captured by the accelerometers the de-noise capabilities of wavelets[18] are used. Additionally, the system behavior with backlash is analyzed through the pseudo phase space (PPS).[6]

### *3.1. The wavelet transform*

The continuous wavelet transform (CWT) is a generalization of the windowed Fourier transform (WFT). The concept of the WFT is very simple. We multiply the signal to be analyzed $x(t)$, by a moving window $g(t-\tau)$, and then we compute the Fourier transform of the windowed signal $x(t)\ g(t-\tau)$. Each FT gives a frequency domain "slice" associated with the time value at the window center. Wavelet analysis is performed in a similar way, in the sense that the signal is multiplied by a function called wavelet. However, in the CWT the width of the "window" changes as the transform is computed. Considering the wavelet function $\psi$ centered at time $\tau$ and scaled by $s$, the CWT of the signal $x(t)$ is

https://doi.org/10.1017/S0263574710000056 Published online by Cambridge University Press

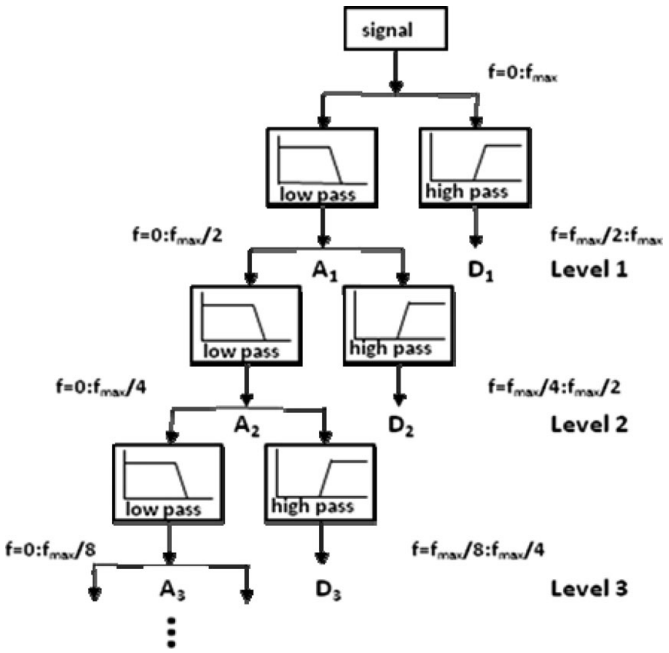


Fig. 2. Simplified diagram of a signal wavelet multiresolution analysis.

represented analytically by

$$CWT(s,\tau) = \frac{1}{\sqrt{|s|}} \int_{-\infty}^{+\infty} x(t)\psi\left(\frac{t-\tau}{s}\right) \mathrm{d}t. \qquad (1)$$

The CWT of the signal $x(t)$ is a function of two variables: translation $\tau$, which corresponds directly to time, and scale/dilation $s$, which indirectly relates to frequency information. The transforming function $\psi(t)$ is called mother wavelet, and consists in a prototype for generating the other window functions. The scale $s$, in the wavelet transform, is similar to the scale used in maps. High scales give a global view of the signal corresponding, in the frequency domain, to the low frequencies. Low scales give detailed information of a signal corresponding, in the frequency domain, to the high frequencies.

The digital version of the CWT is the discrete wavelet transform (DWT) that is considerably faster to implement in a computer. A time-scale representation of a digital signal can also be implemented using digital filtering techniques. An efficient way to implement the DWT using filters was developed by Mallat.[19] Filters of different cutoff frequencies are used to analyze the signal at different scales (see Fig. 2). The signal is passed through a bank of high pass filters to analyze the high frequencies giving detailed information ($D_n$). Additionally, the signal is passed through a bank of low pass filters to analyze the low frequencies giving a coarse approximation ($A_n$). Then the decomposition of the signal into different frequency bands is obtained by successive high-pass and low-pass filtering of the time domain signal.

In what concerns to the wavelet function $\psi(t)$ there is a wide variety of wavelet families, proposed by different researchers, that includes the Haar, Daubechies, Mexican Hat, and Morlet wavelets. The function $\psi(t)$ should reflect the type of features present in the time series.[20] Therefore, the wavelet adopted in this paper is the Haar (Eq. (2)) function due also to its simplicity and small computational time.

In this work we use the signal processing capabilities of the DWT for de-noising the experimental signals:

$$\psi(t) = \begin{cases} 1 & 0 \le t < 1/2, \\ -1 & 1/2 \le t < 1, \\ 0 & otherwise. \end{cases} \qquad (2)$$

### *3.2. The pseudo phase plane*

The PPS is used to analyze signals with nonlinear behavior. For the two-dimensional case it is called pseudo phase plane (PPP).[6,21,22] The proper time lag $T_d$, for the delay measurements, and the adequate dimension $d \in \mathrm{N}$ of the space must be determined in order to achieve the phase space. In the PPP the measurement $s(t)$ forms the *pseudo* vector $y(t)$ according to

$$y(t) = [s(t), s(t+T_d), \ldots, s(t+(d-1)T_d)]. \qquad (3)$$

The vector $y(t)$ can be plotted in a $d$-dimensional space forming a curve in the PPS. If $d=2$ we have a two-dimensional time delay space.

The procedure of choosing a sufficiently large $d$ is formally known as embedding and any dimension that works is called an embedding dimension $d_E$. The number of measurements $d_E$ should provide a phase space dimension, in which the geometrical structure of the plotted PPS is completely unfold, and where there are no hidden points in the resulting plot.

Among others,[21] the method of delays is the most common method for reconstructing the phase space. Several techniques have been proposed to choose an appropriate time delay.[22] One line of thought is to choose $T_d$ based on the correlation of the time series with its delayed image. The difficulty of correlation to deal with nonlinear relations leads to the use of the mutual information. This concept, from the information theory,[23] recognizes the nonlinear properties of the series and measures their dependence. The average mutual information for the two series of variables $t$ and $t+T_d$ is given by

$$I_{av}(t, t+T_d) = \int_t \int_{t+T_d} F_1\{s(t), s(t+T_d))\} \log_2 \times \frac{F_1\{s(t), s(t+T_d)\}}{F_2\{s(t)\}F_3\{s(t+T_d)\}} \mathrm{d}t\,\mathrm{d}(t+T_d), \qquad (4)$$

where $F_1\{s(t),\ s(t+T_d)\}$ is a bidimensional probability density function and $F_2\{s(t)\}$ and $F_3\{s(t+T_d)\}$ are the marginal probability distributions of the two series $s(t)$ and $s(t+T_d)$, respectively.

The index $I_{av}$ allows us to obtain the time lag required to construct the PPS. For finding the best value $T_d$ of the delay, $I_{av}$ is computed for a range of delays and the first minimum is chosen. Usually, $I_{av}$ is referred[6,21,22] as the preferred alternative to select the proper time delay $T_d$.

https://doi.org/10.1017/S0263574710000056 Published online by Cambridge University Press

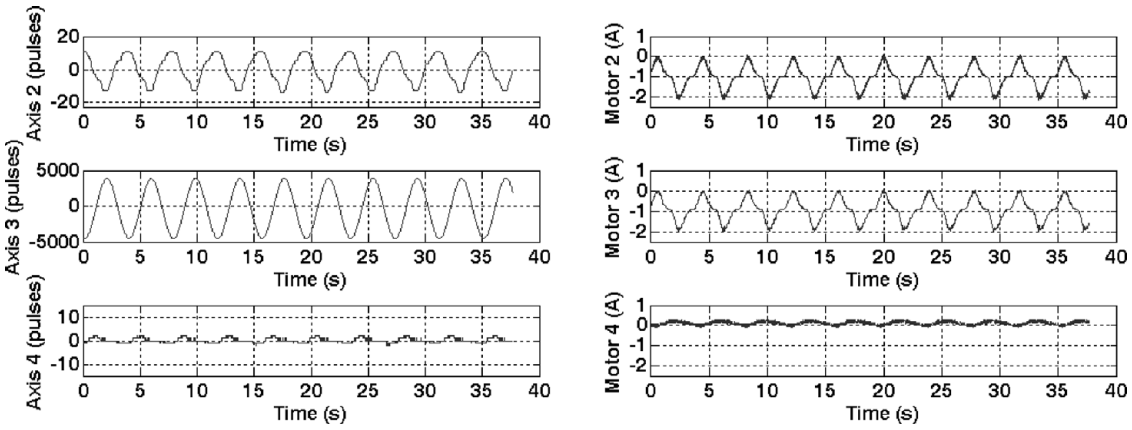


Fig. 3. Robot axis positions for joints 2–4 for the case (iii) (left) and electrical currents of robot axis motors 2–4 for the case (iii) (right).

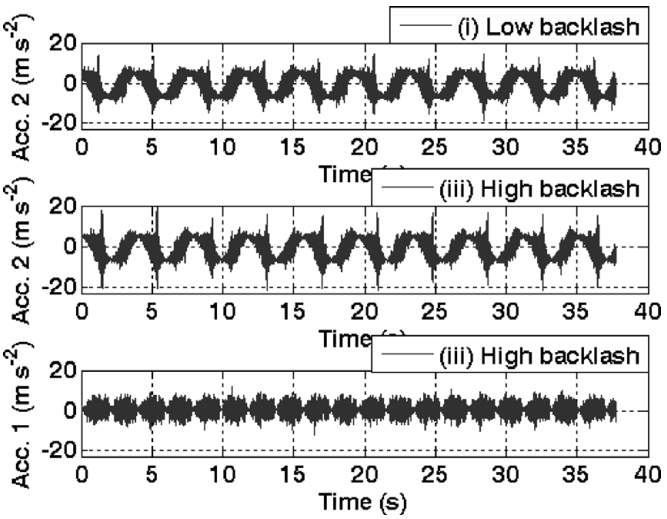


Fig. 4. Signals of accelerometer 1 (bottom) and accelerometer 2 (middle and top).

## 4. Results

According to the platform described in Section 2 we adopt an experiment in which the robot arm moves as a consequence of the joint 3 rotation. By other words, the robot motion is programmed in a way such that only the joint 3 is driven and consequently it oscillates over a predefined range from the vertical position.

Figures 3 and 4 present a typical time evolution of several variables. All the captured robot signals were studied but, due to space limitations, only the most relevant are depicted in this paper.

Figure 3 (left) shows the axis positions of joints 2–4 for the case of high backlash. It is actuated only the joint 3 but, due to the dynamic coupling, the adjacent joints 2 and 4 oscillate slightly. Figure 3 (right) depicts the electrical currents of robot axis motors 2–4 for the high backlash (case (iii)). The currents of the motors reveal the action of the robot control system ensuring the position control.

Figure 4 (middle and bottom) shows the robot accelerations for the case (iii). As referred previously, the accelerometers 1 and 2 are mounted in the end of the upper arm and forearm, respectively (see Fig. 1). The signals from the accelerometers present a considerable noise and it is difficult to extract information about the backlash effect. Several tests demonstrated that the effects of the adjusted backlash are captured only by the accelerometer 2. The signals from the others sensors present significant less noise, but the backlash effect is not observed by them. A priori the accelerometers constitute sensors that are more prone to capture the backlash effect, but the truth is that the accelerometer 1 revealed to be useless due to the high level of noise.

Figure 4 (top and middle) depicts the signal from the accelerometer 2 for the cases (i) and (iii), respectively. The signal corresponding to the case (iii) exhibits larger peaks compared with the case (i). In spite of this detail, the effect of the backlash becomes difficult to analyze due to the amount of noise of the acceleration signals. Therefore, the signals must be filtered in order to reduce the noise. First, it was tried a low-pass Butterworth filter with different cutoff frequencies. The resulting filtered signal presented a noise reduction, but the backlash effect was also reduced. As an alternative the wavelets were adopted. Preliminary tests, with several wavelet families, were performed to verify their capabilities. The Haar wavelet revealed good results and was adopted due to its simplicity and low computational time.

Figure 5 depicts the wavelet decomposition tree with the resulting frequency bands of the corresponding approximation ($A_n$) and detail ($D_n$) components for each level. Since the sampling rate of the captured signal is 750 Hz, the frequency ranges are approximately the values shown in the diagram.

Figure 6 (left) shows the five level components obtained through the process of decomposition of the accelerometer 2 signal in the case (i). The original signal captured from the accelerometer 2 is shown at the top. The approximation component reveals the low frequency part of the acceleration 2. The five detail components show the high-frequency parts for the different frequency bands. A method of filtering based on the threshold level for each component is used. For the distinct components the values adopted for the threshold level, based on an experimental procedure, are [3.74, 4.42, 4.26, 4.09, 3.92, 3.74] $ms^{-2}$ for the wavelets components $[A_5, D_1, D_2, D_3, D_4, D_5]$, respectively. Figure 6 (right) shows at the top the resulted

https://doi.org/10.1017/S0263574710000056 Published online by Cambridge University Press

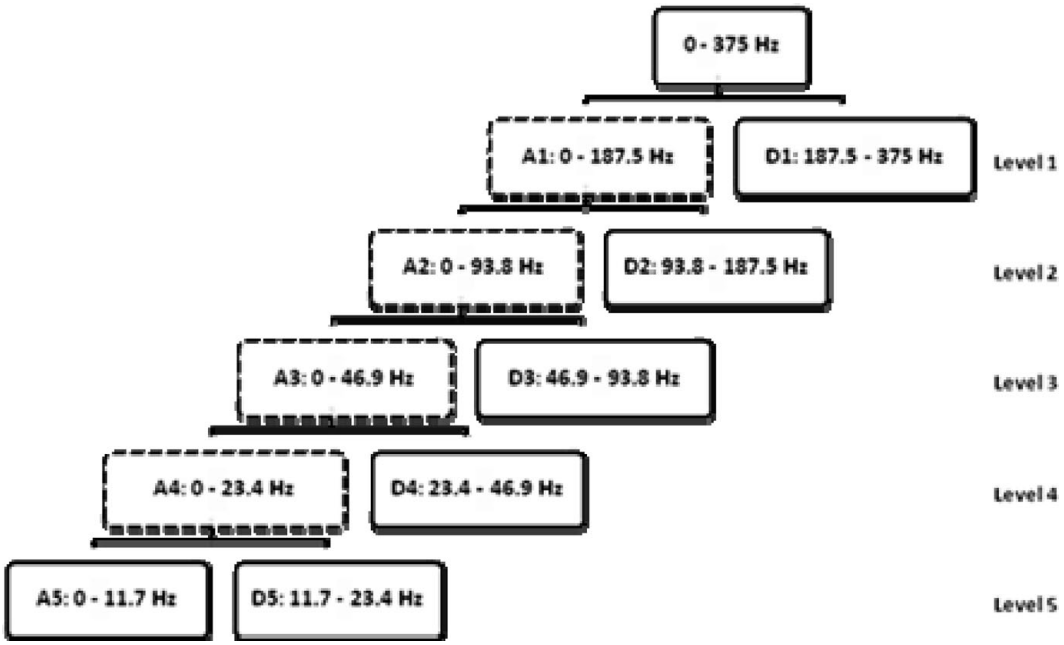


Fig. 5. Wavelet decomposition and the resulting frequency bands

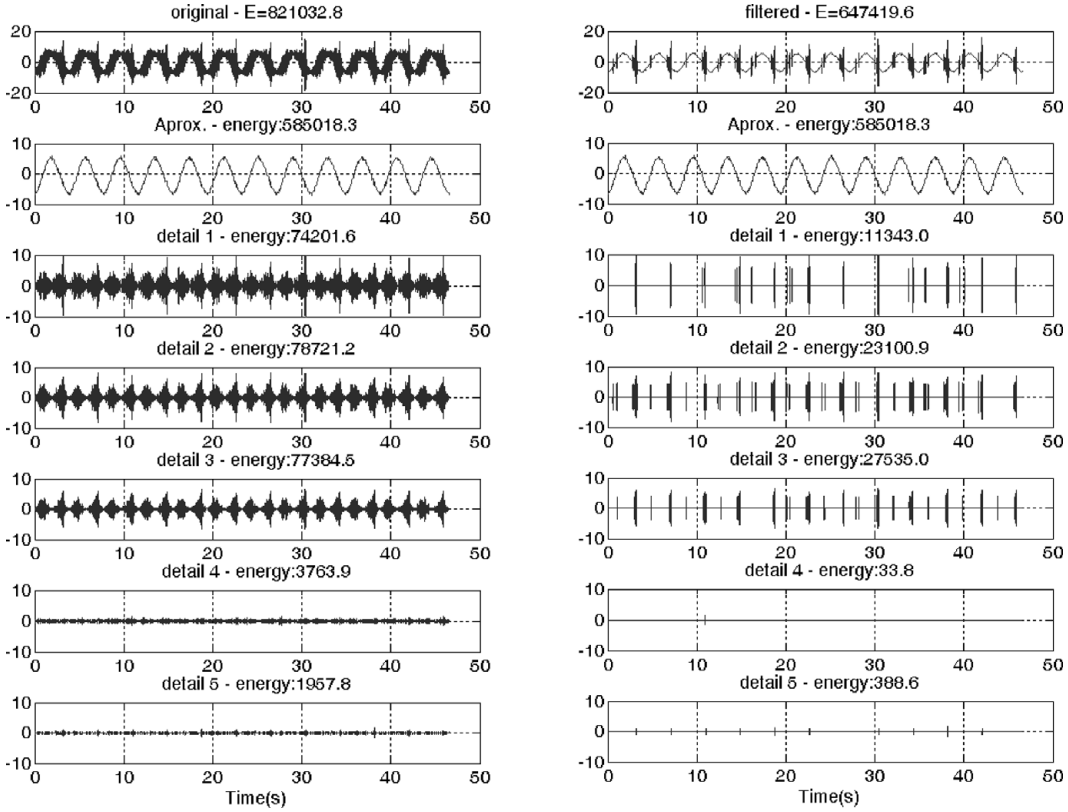


Fig. 6. Wavelet decomposition of the accelerometer 2 signal for the case (i): noisy (left); filtered (right).

filtered signal where it is evident the effect of the backlash. Figure 6 (right) shows also the six components of the filtered signal, corresponding to the same frequency bands shown in the left. Comparing the five detail components of the filtered signal, with those ones from the original signal, it is clear the effect of filtering. Additionally, the energy values of each wavelet component are shown in Fig. 6. Comparing the filtered with the noisy signal reveals that the process of filtering removes about 21% of the signal energy.

To compare the wavelet transforms energies of each level, the normalized values are adopted. Therefore the total energy resulted from the sum of all the signal components is the unity. Figure 7 depicts the normalized energy for the six components resulted from the decomposition process. The distribution of the energy in the frequency domain is not uniform. The signal has the energy concentrate at low frequency, namely at $A_1$ component. Nevertheless, the signal has also a significant amount of energy at $D_1$ to $D_3$ details.

https://doi.org/10.1017/S0263574710000056 Published online by Cambridge University Press

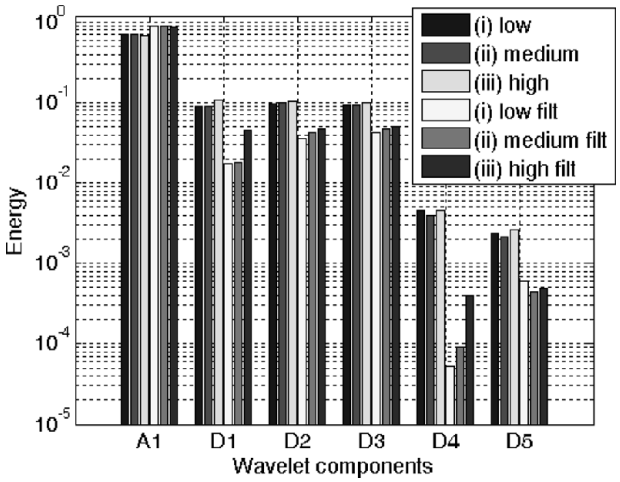


Fig. 7. Wavelet components energy of the accelerometer 2 original and filtered signals for the three cases.

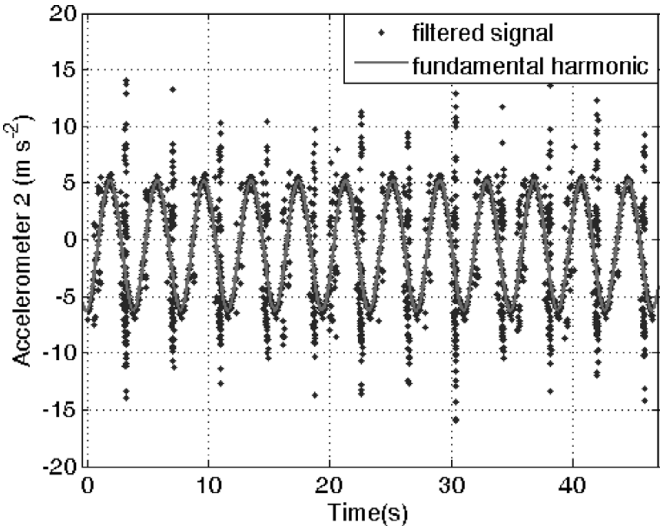


Fig. 8. Filtered accelerometer 2 signal and its fundamental harmonic for the case (i).

In terms of energy, the approximation component $A_1$ is the most important, either for the noisy signal or for the filtered signal. However, the $A_1$ component is not sensitive to the backlash. Additionally, the details $D_1$ of the noisy signal for the cases (i), (ii), and (iii) have the same energy approximately, while for the filtered signal, the component energy for the three cases varies significantly. The detail components $D_2$ and $D_3$ present a similar behavior to the one described for the component $D_1$. Therefore, comparing the $\{D_1, D_2, D_3\}$ details we can say that these components of the noisy signal are not sensitive to the backlash while the filtered versions components changes with the backlash. For the noisy signal, the detail components $\{D_4, D_5\}$ present identical energy, while for the filtered signal the corresponding components energy for the three cases is negligible.

In conclusion, we can say that the approximation component $A_1$ is the signal responsible for the excitation of the system, while the $\{D_1, D_2, D_3\}$ details of the filtered signal are the components sensitive to the backlash. Finally, the detail components $\{D_4, D_5\}$ are essentially noise.

The filtered periodic signal can be expanded to a Fourier series in the form

$$x_{FS}(t) = a_0 + \sum_{k=1}^{\infty} [a_k \cos(k\omega t) + b_k \sin(k\omega t)]. \quad (5)$$

An infinite number of terms (i.e. the fundamental term and the harmonics) are required to fit the filtered signal $x(t)$ with $x_{FS}(t)$. However, we can assume that the filtered signal $x(t)$ (see Fig. 6 right at top) is composed by the fundamental harmonic perturbed by the backlash effect. Therefore, for the low backlash (case (i)), with $k = 1$, we obtain $(a_0, a_1, b_1) = (-0.53, -5.69, 0.72)$. Figure 8 shows the filtered accelerometer 2 signal for the case (i) and its fundamental harmonic.

Figure 9 depicts the PPPs of the noisy and filtered accelerometer 2 signals, for the experiment with the low and high backlash, and the fundamental harmonic. As referred previously, usually the time lag adopted for the PPS is based on the correlation or mutual information of the time series. In this work, practice reveals that the best time lag is that one corresponding to one quarter of the period of the fundamental harmonic, which was adopted for the PPPs shown in Fig. 9. Once again, we observe the advantages of filtering the signal. Comparing the PPPs of the noisy signal for the cases (i) (Fig. 9a) and (iii) (Fig. 9b) we can see the backlash effect; however, due to noise it is difficult to measure it. This task is simplified using the corresponding PPPs for the filtered signal (Fig. 9c–d). In this line of thought was developed a metric based on the error between the filtered signal and its fundamental harmonic to analyze the influence of the distinct levels of backlash in the robotic system. For the two components $x(t)$ and $x(t - \tau)$ of the PPP, the index is based on the root mean square error in discrete time, given by

$$RMSE^2 = RMSE_t^2 + RMSE_{t-\tau}^2, \quad (6)$$

where

$$RMSE_t\{x(t)\} = \frac{\frac{1}{N}\sum_{k=0}^{N}[x(kT) - x_1(kT)]^2}{\frac{1}{N}\sum_{k=0}^{N}x^2(kT)},$$

where $x_1(t)$ is the fundamental harmonic and $T$ is the sampling period.

The *RMSE* values computed for the three cases of backlash using the filtered signal $(RMSE^{\mathrm{i}}, RMSE^{\mathrm{ii}}, RMSE^{\mathrm{iii}}) = (2.24, 2.44, 3.14) \times 10^{-7}$ show that the index magnitude increases with the level of backlash (see Fig. 10). On the other hand, the corresponding values for the unfiltered signal are $(RMSE^{\mathrm{i}}, RMSE^{\mathrm{ii}}, RMSE^{\mathrm{iii}}) = (5.13, 5.09, 5.43) \times 10^{-7}$ which reveals a different behavior due to the effect of noise. Additionally, a set of experiments were developed to study the influence of the amplitude and frequency of the joint 3 motion upon the backlash dynamics. Figure 11 depicts the *RMSE* of the accelerometer 2 signal for the nine experiments.

https://doi.org/10.1017/S0263574710000056 Published online by Cambridge University Press

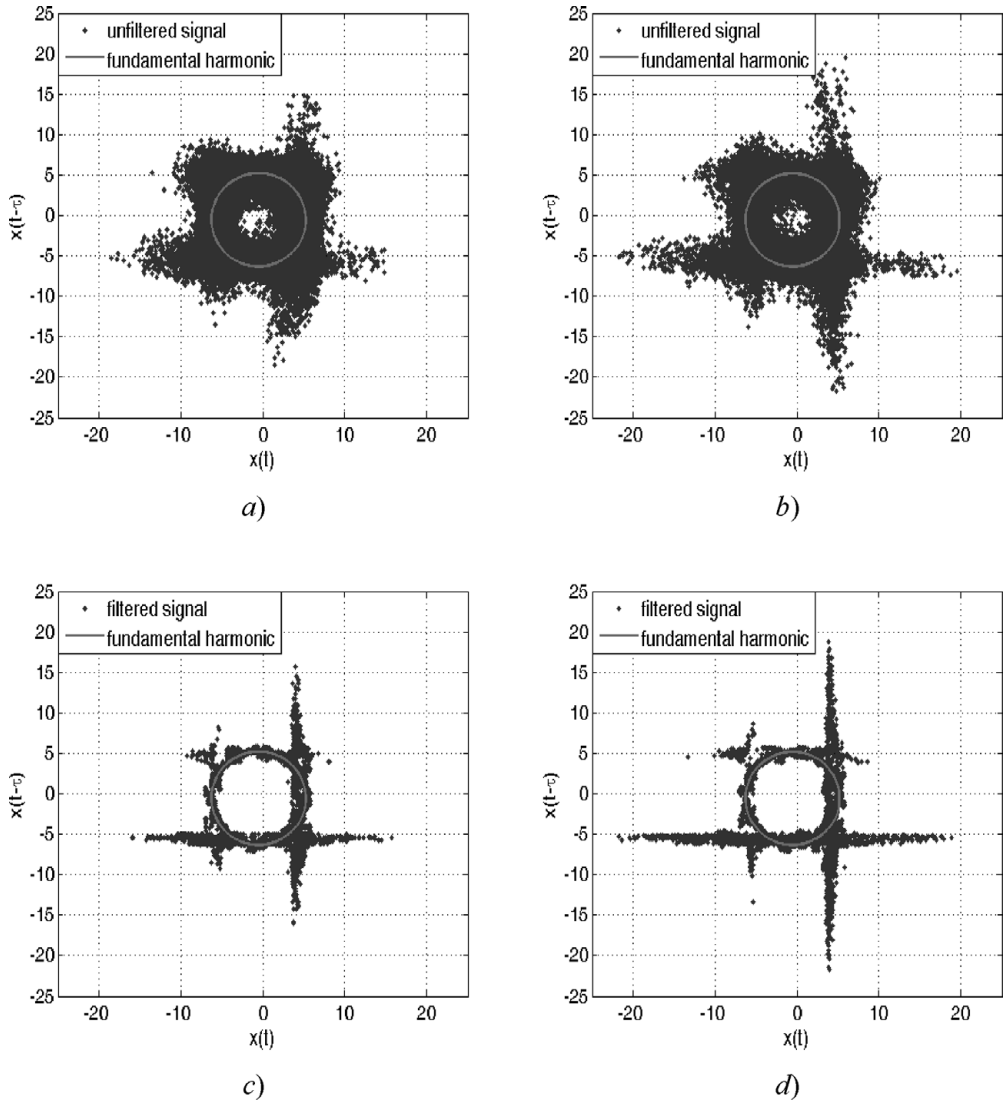


Fig. 9. PPPs of the accelerometer 2 signal and its fundamental harmonic: (a) noisy signal for the case (i); (b) noisy signal for the case (iii); (c) filtered signal for the case (i); (d) filtered signal for the case (iii).

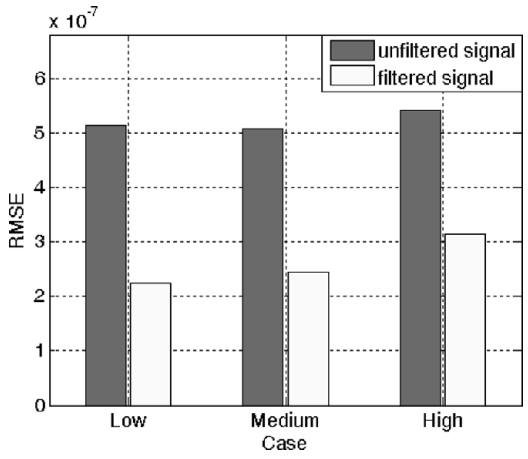


Fig. 10. *RMSE* for noisy and filtered versions of the accelerometer 2 signal for the three cases.

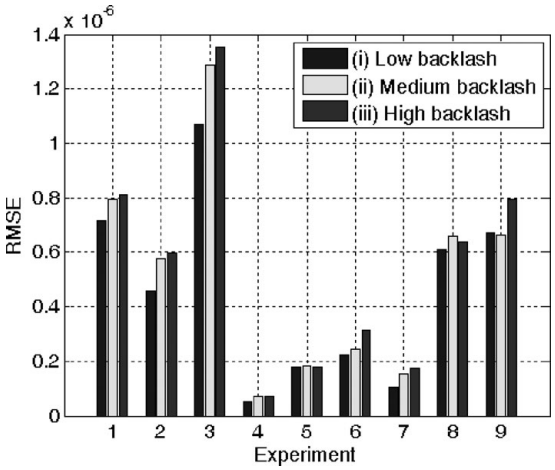


Fig. 11. RMSE of the accelerometer 2 signal for a set of experiments: cases (i), (ii), and (iii).

The results confirm, in general, the behavior of the *RMSE* that increases with the level of the backlash. However, for some experiments, the index is not in complete accordance with the expected results. This fact can be caused by the noise of the signal that is not filtered completely, probably due to the method adopted for the selection of the threshold level.

https://doi.org/10.1017/S0263574710000056 Published online by Cambridge University Press

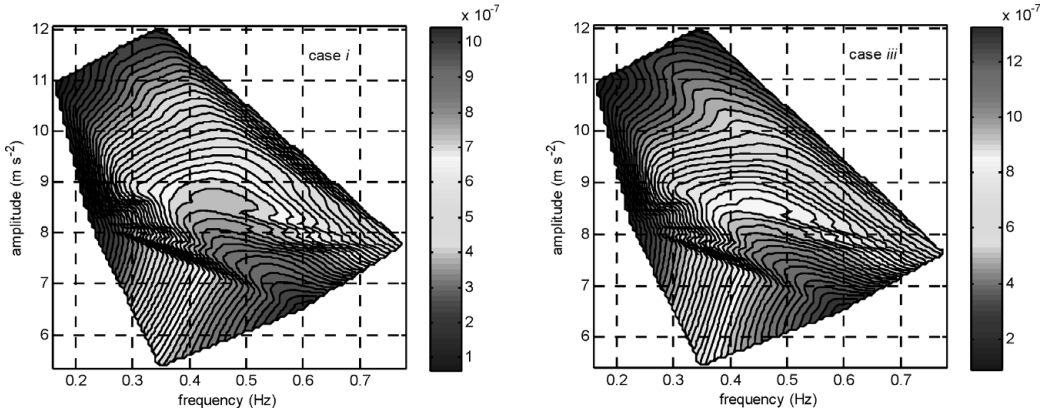


Fig. 12. RMSE of the accelerometer 2 signal vs. amplitude and frequency of joint 3 movements.

The use of another method (e.g. an heuristic one) or the use of another type of wavelet, could mitigate the problem of the noise. A deeper insight into the nature of this problem must be envisaged.

Additionally, Fig. 12 (left) depicts the *RMSE* values of the accelerometer 2 signal *vs* the amplitude and frequency of joint 3 movements for low backlash case. The nine points, shown in Fig. 11 for each individual case, produce a smooth surface that relates the three variables. There is a maximum of *RMSE* $1.06 \times 10^{-6}$ that occurs at (frequency, amplitude) = (0.6, 6.5). Figure 12 (right) depicts the same variables for the high backlash case and we verify that we have a *RMSE* = $1.35 \times 10^{-6}$ maximum that occurs again at (frequency, amplitude) = (0.6, 6.5).

The tests developed in this article proved that the *RMSE* reveals to be a good index for the backlash analysis.

## 5. Conclusions

The tests demonstrate the usefulness of the wavelets on filtering the experimental signals reducing the noise while maintaining important features about the backlash. The energy analysis of the signals revealed the components responsible for the excitation of the system and for the backlash.

An index based on the PPP was proposed to detect the backlash effect on a robotic manipulator. The tests proved that the RMSE is an appropriate index for the backlash analysis.

In a future work, we plan to pursue several researches in order to further understand the backlash phenomenon. These include the study of the wavelet tuning parameters, in the process of de-noising, and the analysis of the backlash with various static preloads applied on the robot end-effector.

## References

1. N. G. Dagalakis and D. R. Myers, "Adjustment of robot joint gear backlash using the robot joint test excitation technique," *Int. J. Robot. Res.***4**(2), 65–79 (1985).
2. J. L. Stein and C.-H. Wang, "Automatic detection of clearance in mechanical systems: Theory and simulation," *Proc. Am. Control Conf.* **3**, 1737–1745 (1995).
3. N. Sarkar, R. E. Ellis and T. N. Moore, "Backlash detection in geared mechanisms: modeling, simulation, and experimentation," *Mech. Syst. Signal Process.* **11**(3), 391–408 (1997).
4. G. Hovland, S. Hanssen, S. Moberg, T. Brogårdh, S. Gunnarsson and M. Isaksson, "Nonlinear Identification of Backlash in Robot Transmissions," *Proceedings of the 33rd International Symposium on Robotics* (ISR 2002), Stockholm, Sweden (Oct. 7–11, 2002). Paper in CD-Rom proceedings.
5. R. Merzouki, J. A. Davila, J. C. Cadiou and L. Fridman, "Backlash Phenomenon Observation and Identification," *Proceedings of American Control Conference*, Minneapolis, MN (2006) pp. 3322–3327.
6. I. Trendafilova and H. Van. Brussel, "Non-linear dynamics tools for the motion analysis and condition monitoring of robot joints," *Mech. Syst. Signal Process*. **15**(6), 1141–1164 (Nov. 2001).
7. A. Azenha and J. A. T. Machado, "Variable Structure Control of Robots with Nonlinear Friction and Backlash at the Joints," *Proceedings of the IEEE International Conference on Robotics and Automation*, Minneapolis, USA (1996) pp. 366–371.
8. M. Nordin and P.-O. Gutman, "Controlling mechanical systems with backlash – A survey," *Automatica* **38**, 1633–1649 (2002).
9. C. Ma and Y. Hori, "The Application of Fractional Order Control to Backlash Vibration Suppression," *Proceedings of American Control Conference*, Boston, MA (2004) pp. 2901–2906.
10. M. Nordin and P.-O. Gutman, "Non-Linear Speed Control of Elastic Systems with Backlash," *Proceedings. 39th IEEE Conf. on Decision and Control*, Sydney, Australia (Dec. 2000) pp. 4060–4065.
11. David R. Seidl, Sui-Lun Lam, Jerry A. Putman and Robert D. Lorenz, "Neural network compensation of gear backlash hysteresis in position-controlled mechanisms," *IEEE Trans. Ind. Appl.* **31**, 1475–1483 (6 Nov./Dec., 1995).
12. C.-Y. Su, M. Oya and H. Hong, "Stable adaptive fuzzy control of nonlinear systems preceede by unknown backlash-like hysteresis," *IEEE Trans. Fuzzy Syst.* **11**(1), 1–8 (Feb. 2003).
13. Z. Shi, Y. Zhong, W. Xu and M. Zhao, "Decentralized Robust Control of Uncertain Robots with Backlash and Flexibility at Joints," *IEEE/International Conference on Intelligent Robots and Systems*, Beijing, China (2006) pp. 4521–4526.
14. K. Xu and N. Simaan, "Actuation Compensation for Flexible Surgical Snake-like Robots with Redundant Remote Actuation," *IEEE Conf. on Robotics and Automation*, Orlando, FL (2006) pp. 4148–4154.
15. E. J. Park and J. K. Mills, "Static shape and vibration control of flexible payloads with applications to robotic assembly," *IEEE/ASME Trans. Mechatronics* 6, **10**, 675–687 (2005).
16. T. Mouri, H. Kawasaki and K. Umebayashi, "Developments of new anthropomorphic robot hand and its master slave system," *IEEE IROS* 3225–3230 (2005).
17. M. F. M. Lima, J. A. T. Machado and M. Crisóstomo, "Experimental set-up for vibration and impact analysis in robotics," *WSEAS Trans. Syst.* **4**(5), 569–576 (May, 2005).

https://doi.org/10.1017/S0263574710000056 Published online by Cambridge University Press

18. S. Mallat, *A Wavelet Tour of Signal Processing*, 2nd ed. (Academic Press, London, UK, 1999).
19. S. Mallat, "A theory for multiresolution signal decomposition: The wavelet representation," *IEEE Trans. Pattern Anal. Mach. Intell.* **11**(7), 674–693 (1989).
20. C. Torrence and G. P. Compo, "A practical guide to wavelet analysis," *Bull. Am. Meteorol. Soc.* **79**(1), 61–78 (1998).
21. B. F. Feeny and G. Lin, "Fractional derivatives applied to phase-space reconstructions, special issue on fractional calculus," *Nonlinear Dyn.* **38**(1–4), 85–99 (2004).
22. Henry D. I. Abarbanel, Reggie Brown, John J. Sidorowich and Lev Sh. Tsimring, "The analysis of observed chaotic data in physical systems," *Rev. Mod. Phys.* **65**(4), 1331–1392 (1993).
23. C. E. Shannon, "A mathematical theory of communication," *Bell Syst. Tech. J.* **27**, 379–423; 623–656 (July, Oct. 1948).

https://doi.org/10.1017/S0263574710000056 Published online by Cambridge University Press